Electrochimica Acta 174 (2015) 508–515

Contents lists available at ScienceDirect

Electrochimica Acta

journal homepage: www.elsevier.com/locate/electacta

A nanostructured bifunctional Pd/C gas-diffusion electrode for metal-air batteries

R.D McKerracher[a], C. Alegre[b], V. Baglio[b], A.S. Aricò[b], C. Ponce de León[a,*], F. Mornaghini[c], M. Rodlert[c], F.C. Walsh[a]

[a] Electrochemical Engineering Laboratory, Engineering Sciences, University of Southampton, Highfield, Southampton, SO17 1BJ, UK
[b] Consiglio Nazionale delle Ricerche, Istituto di Tecnologie Avanzate per l'Energia " Nicola Giordano", Salita S.Lucia sopra Contesse, 5. 98126 Messina, Italy
[c] Imerys Graphite & Carbon, Strada Industriale- 12, CH - 6743 Bodio, Switzerland

ARTICLE INFO

Article history:
Received 9 March 2015
Received in revised form 15 May 2015
Accepted 1 June 2015
Available online 3 June 2015

Keywords:
bifunctional air electrode
palladium catalyst
metal-air battery

ABSTRACT

Designing a bifunctional air electrode which catalyses both the oxygen reduction and oxygen evolution reactions is an essential part of progress towards fully rechargeable metal-air batteries, such as the iron-air battery which is environmentally friendly, low cost, and does not suffer risk of thermal runaway like lithium-ion batteries. This paper reports the development of a lightweight carbon-based bifunctional air electrode, catalysed by a small (0.5 mg cm^{-2}) loading of 30 wt.% palladium on carbon. The Pd-catalysed air electrode showed good bifunctional activity, with 0.53 V potential difference between oxygen reduction and evolution. The Pd/C air electrode showed improved catalytic activity at high current densities ($\geq$ 50 mA cm^{-2}) and enhanced durability compared with two commercial Pt/C air electrodes produced by Gaskatel GmbH and Johnson Matthey. A stable oxygen evolution potential was maintained over 1,000 charge-discharge cycles.

1. Introduction

Metal-air batteries are currently of great research interest, particularly in the area of rechargeable batteries for electric vehicles [1]. This is because they use atmospheric oxygen as a source of energy, which allows the batteries to be lightweight as only a thin, low-density "air breathing" cathode is needed to catalyse the oxygen reactions. The anode can be made from a variety of metals, for example zinc, iron, aluminium or lithium. Heavy metals can be avoided entirely or used only in small amounts (e.g. 5 wt.%), giving the metal-air batteries a considerably lower density than lead acid batteries. The theoretical specific energy density of a metal-air battery (up to 12,000 W h kg^{-1}) [2] is much greater than the energy density of the lithium-ion batteries currently used in rechargeable vehicles (up to 1,000 W h kg^{-1}) [2], and metal-air batteries do not suffer from the thermal runaway safety issues of lithium-ion batteries [3].

One of the greatest challenges is to make a rechargeable metal-air battery that can be re-used for thousands of charging and discharging cycles. In terms of the choice of anode, iron-air batteries may be most suitable, because iron is less easily corroded than aluminium or lithium, and does not suffer the dendrite formation problems of zinc-air batteries during re-charging [4]. The air breathing cathode of a rechargeable iron-air battery also needs to be able to support repeated cycling without substantial degradation in performance.

A rechargeable air cathode must have good bifunctionality, i.e. be able to reduce oxygen during discharge and evolve oxygen during charge. The most efficient and cost-effective way of achieving this is to include a single bifunctional catalyst in the electrode, rather than one catalyst for each separate reaction. However, in practice, separate electrocatalysts are often used for the two reactions of the bifunctional electrode [5] because good bifunctional oxygen catalysts are rare, and often involve precious metals such as platinum and palladium. These metals and their alloys need to be used sparingly, or cheaper alternatives such as perovskites [6,7] or spinels [8–10] can be used.

Palladium oxygen catalysts have been reported in a number of studies, [11–17] A wide range of palladium loadings and particle sizes have been studied, and compared with state-of the-art platinum catalysts. A study performed in 1983 suggested that the catalytic activity per gram of platinum and palladium supported on graphite is similar if the metals are highly dispersed, i.e. the loading is small ($<$2 atomic% or $<$33 wt% in the catalyst layer), [15]. Another study suggested superior performance of palladium to platinum if used in a methanol fuel cell cathode with

* Corresponding author.
E-mail address: C.A.Ponce-de-Leon-Albarran@soton.ac.uk (C. Ponce de León).

http://dx.doi.org/10.1016/j.electacta.2015.06.001
0013-4686/

$\leq 2\,mg\,cm^{-2}$ catalyst loading [13]. Superior performance of Pd/C compared with Pt/C was also reported for palladium supported in thin graphite sheets, although the authors did not report the Pd catalyst loading [16]. A recent study from 2015 showed that 30 wt. % Pd supported on Vulcan had higher activity for the oxygen evolution reaction than 30 wt.% Pt on Vulcan, and also had improved durability during repeated cycling tests [17]. These studies provide some justification for using the cheaper palladium instead of platinum in applications where the catalyst loading is low and the catalyst particles are well- dispersed.

In the majority of the above studies the palladium and platinum catalysts were layer-deposited onto small glassy carbon rotating disk electrode, not a complete air electrode with a gas-diffusion layer, and the oxygen reduction reaction alone was studied rather than the bifunctional reactions (charge and discharge). It is apparent in the literature on bifunctional air electrodes in general that although a large number of publications study bifunctional catalysts deposited onto the surface of rotating disk electrodes (RDEs) in oxygen saturated solution (for recent publications see the references [6,18–22]), there is a much more limited number of publications which look at the properties of such catalysts when they are on the surface of complete gas diffusion electrodes [7–9,17,23].

In order to assess the practicality of using a particular catalyst it is important to study not only the characteristics on a RDE, but also *in-situ* on a gas diffusion electrode. This is because the activity of the catalyst is not the only important factor in the construction of a rechargeable air electrode: the interaction of the catalyst with the supporting layers of the electrode and the current collector, and the efficiency of oxygen transport to the catalyst through the gas diffusion layer, are also of importance. For instance, catalysts which appear to have a strong performance on a solid glassy carbon or gold RDE may not have such high activity when adsorbed onto high surface area gas diffusion layer [24].

For this reason, the supporting materials onto which the catalyst materials are absorbed must also be optimised. Carbon is usually the conductive supporting material of choice for air electrode catalysts due to its low density and high surface area. However, carbon has a tendency to undergo corrosion during repeated current cycling on an air electrode, particularly during the charging process where the air electrode is at positive (oxidising) potentials. The products of this corrosion process are oxygen-functionalised carbon such as $-COO^{-}$, or carbonates CO_3^{2-} formed via CO_2 generation [25,26]. As the carbon corrodes, oxidised particles may detach and dissolve into the electrolyte, leading to the loss of carbon and catalyst particles from the air electrode surface and a decrease in the electrochemical surface area [27,28]. The performance of carbon-based gas diffusion electrodes will therefore deteriorate over time. The development of carbon supporting materials with high corrosion resistance is vital to ensure that air electrodes have a good durability over many charge-discharge cycles.

This paper outlines the development of a palladium-catalysed bifunctional air-breathing electrode, and demonstrates how obtaining a good dispersion of palladium nanoparticles can create a stable catalyst with good activity at low catalyst loadings, such that only very small quantities ($0.5\,mg\,cm^{-2}$) of palladium are sufficient to give good performance. The choice of carbon materials and their role in ensuring the long-term durability of the air electrode are also discussed.

2. Experimental Details

2.1. Synthesis and characterisation of the Pd/C catalyst

The Pd catalyst was synthesized by means of a colloidal method, employing sulphites as complexing agents, as described elsewhere [29,30]. The carbon support (supplied by Imerys Graphite & Carbon, $220\,m^2\,g^{-1}$ specific surface area, subsequently referred to in this paper as C) was suspended in distilled water and stirred in an ultrasonic water bath at about 80 °C to form a slurry. An acidic solution containing an appropriate amount (to reach a final loading of 30 wt.% of Pd on the support) of $Na_6Pd(SO_3)_4$ was successively added to the slurry. The Pd sulphite complex solution was decomposed by adding H_2O_2 and successively increasing the pH to 5.5 to form colloidal PdO_x/C. The metallic oxide was reduced in a H_2 stream at room temperature (23 °C) to form the 30 wt.% Pd/C catalyst.

The catalysts were characterized by X-ray diffraction (XRD) using a Philips X-pert 3710 X-ray diffractometer with Cu Kα radiation operating at 40 kV and 30 mA. The peak profile of the (220) reflection in the face centred cubic structure of Pd was analysed by using the Marquardt algorithm, and it was used to calculate the crystallite size by the Debye-Scherrer equation. Transmission electron microscopy (TEM) analysis was made by first dispersing the catalyst powder in isopropyl alcohol. A few drops of this solution was deposited on carbon-film-coated Cu grids and analysed with a FEI CM12 microscope. The total metal content in the catalysts was determined by burning the carbon support in a thermal gravimetric experiment up to 950 °C in air.

Cyclic voltammetry was also performed in order to calculate the electrochemically active surface area (ESA) of the catalyst. A cell with a three-electrode assembly and an Autolab potentiostat-galvanostat were used to carry out the electrochemical characterization. The working electrode consisted of a thin layer of the catalyst deposited on a pyrolytic graphite disk (5 mm) polished to a mirror finish using an alumina suspension. The counter electrode consisted of a high surface Pt wire and the reference electrode was an Hg/HgO electrode filled with a $1\,mol\,dm^{-3}$ KOH solution (AMEL Electrochemistry, - 115 mV vs. SHE). An aqueous suspension consisting of $1\,mg\,cm^{-3}$ of the Pd/C catalyst was obtained by ultrasonically dispersing it in iso-propanol and Nafion ionomer (30 wt.%) (purchased from Ion Power). The Pd loading on the working electrode was $50\,\mu g\,cm^{-2}$. After preparation, the electrode was immersed into deaerated $1\,mol\,dm^{-3}$ KOH electrolyte, prepared from high purity reagents (Sigma–Aldrich) and ultrapure water. Cyclic voltammograms were carried out at scan rate of $20\,mV\,s^{-1}$, between −0.93 and 0.27 V vs. Hg/HgO (0 and 1.2 V vs. RHE). All the experiments were carried out at room temperature. The ESA was determined from the integration of the current involved in the reduction of the palladium oxide assuming $405\,\mu C\,cm^{-2}$ for the reduction of a monolayer of PdO_x and correcting by the double layer capacitance [31].

2.2. Construction of the gas diffusion electrode

The Pd/C gas diffusion electrode was composed of three main parts: a gas diffusion layer, a catalyst layer, and a current collector, which were bound together in a single step by hot-pressing. To make the gas diffusion layer, a carbon cloth of 0.11 mm thickness treated with 25 wt.% PTFE was purchased from FuelCell.com, and cut into a 5×5 cm piece. A paste was made from 80 wt.% of a $64\,m^2g^{-1}$ low-surface area carbon (supplied by Imerys Graphite & Carbon, subsequently referred to in this paper as C1) mixed with 20 wt.% PTFE (DISP 30 solution, DuPont) and 10 cm^3 water per 1 g of solids. The paste was then rolled evenly over the carbon cloth to a thickness of approximately 100 μm.

To make the catalyst layer, the 30 wt. % Pd/C catalyst was sonicated for 15 minutes in a 5 wt.% Nafion ® solution in aliphatic alcohols (Sigma Aldrich), in a weight ratio of 3:2 for the catalyst: Nafion. The sonication resulted in a black viscous ink. The catalyst layer ink was spread evenly on top of the gas diffusion layer (which was not allowed to dry out, to prevent it from detaching from the

carbon cloth before pressing). The mass of the 30 wt.% Pd/C catalyst was measured to give a 0.5 mg cm^{-2} loading of Pd (i.e. a 1.67 mg cm^{-2} loading of the catalyst) on the surface of the electrode.

Finally, a piece of expanded nickel mesh (Dexmet, 32 mesh, 0.05 mm thick) was cut to size and placed on top of the catalyst layer. The air electrode was placed in a hydraulic press (Carver, model 3851) whilst still slightly wet and pressed for 2 minutes at 180 °C temperature, and 5 MPa pressure. The electrode was coated in non-stick silicone grease-proof paper to prevent it from adhering to the plates of the hot press. The electrode was removed carefully from the press and left to cool down to room temperature (20 °C).

2.3. Electron microscopy of gas diffusion electrode

Scanning electron microscopy was performed on a JSM 6500F thermal emission scanning electron microscope with an accelerating voltage of 0.5 - 30 kV. The same instrument was used to record the EDX spectra.

2.4. Electrochemical analysis of gas diffusion electrode

An Autolab potentiostat (Metrohm, model PGSTAT 302N) was used for the electrochemical analysis. All of the cyclic voltammograms in 6 mol dm^{-3} KOH were recorded at a scan rate of 1 mV s^{-1}. The electrochemical analysis was performed in a 3-electrode glass cell with a 1 cm^2 platinum mesh counter electrode and an Hg/HgO reference electrode (Hach-Lange Ltd., - 115 mV vs. SHE) filled with a 1 mol dm^{-3} KOH solution. The area of platinum-catalysed air electrode used in each test was 0.785 cm^2. Oxygen flow was added to the back of the air electrode at a rate of 100 cm^3 min^{-1}, with the gas exit open to the atmosphere. To control the temperature, heat was applied to the cell by flowing water from a water pump (Julabo, model F12-EH) around a glass jacket surrounding the cell.

2.5. Electrolyte

The electrolyte was made by dissolving KOH pellets (Fisher Scientific, > 86%) in high purity deionised water (< 10 μS cm^{-1}), to a concentration of 6 mol dm^{-3}. The solution was left to cool to room temperature (20 °C) before use.

2.6. Corrosion testing of the electrode carbon materials

The carbons C and C1were dispersed together with a proton conducting polymer (an ionomer aqueous dispersion) by high-shear mixing using an additional solvent (water and 1,2-propanediol). The ratio polymer: carbon was 0.75 by weight. The dispersion was coated onto a carbon paper support by doctor blading. A heat treatment procedure (up to 190 °C in air) was applied in order to sinter the polymeric particles used as the binder. The final carbon loading was approximately 1 mg cm^{-2}.

An Hg/HgO reference electrode (Koslow Scientific Research) filled with a 1 mol dm^{-3} KOH solution was used for corrosion testing. A graphite rod was used as the counter electrode. The working electrode (coated carbon paper sample) was placed along the wall of the cylindrical vessel, in concentric configuration around the counter electrode. The tip of the reference electrode was placed at a few mm distance from the working electrode.

The carbon mass loss was calculated from the corrosion current flowed after the first 60 s (the initial current flow being ascribed to the charging of the double layer) assuming a four-electron process and expressed as percentage of the carbon mass initially present in the coating. The mass loss was attributed entirely to the carbon present in the coating; blank measurements showed that the contribution of the carbon paper support to the total corrosion current of regular samples was less that 15%, even in the case of the most corrosion-resistant carbon tested.

3. Results and Discussion

3.1. Characteristics of the Pd/C catalyst

The XRD pattern of the carbon-supported 30 wt.% Pd/C catalyst is reported in Fig. 1. The catalyst shows a typical face centered cubic structure (fcc). Line broadening analysis of the (111), (200), (220) and (311) reflection peaks (Fig. 1) indicated a crystallite size of about 4.0 nm, however the (220) peak at around 68° is the only peak without interference with other peaks, so the average crystallite size obtained from this peak, 3.4 nm, should present the most accurate value. The C (002) graphite carbon reflection occurs at approximately 25°. The shape and intensity of this peak indicates that the carbon material presents a partially graphitic structure [32].

TEM analysis (Fig. 2) showed a good dispersion of the metallic palladium nanoparticles on the carbon, and a mean particle size similar to the crystallite size determined by XRD. In the right-hand side TEM image of Fig. 2, the graphitic planes of the carbon support can also be seen. The results of particle size determination of around 200 palladium particles (Fig. 2b) indicates that the majority of the particles (80%) are within 2-5 nm size, which agrees with the average particle size determined by XRD. Thermal gravimetric analysis confirmed the metal concentration of 30 wt.% Pd with an estimated accuracy of ± 1%.

Fig. 3 shows the cyclic voltammogram obtained for the 30 wt. % Pd/C catalyst in a 1 mol dm^{-3} solution of KOH. The Pd/C presents a surface area of 65 m^2 g^{-1}, which is calculated from the area under the reduction peak of the palladium oxide at −0.27 V vs. Hg/HgO (Fig. 3) [33,34]. In the literature, BET surface areas are more commonly presented than electrochemically-determined surface areas, so it is difficult to compare with other bifunctional oxygen catalysts; BET surface areas of 11 m^2 g^{-1} for $LaNiO_3$ [35], 10 m^2 g^{-1} for IrO_2/Ti, [36] and 16-38 m^2 g^{-1} for Co_3O_4 spinel [37] catalysts are given, so a surface area of 65 m^2 g^{-1} seems very reasonable for an active bifunctional catalyst.

The physical properties of the carbon support material, C, as well as the gas-diffusion layer carbon C1, are shown in Table 1. The carbon support material in Pd/C had a higher surface area than C1 to allow sufficient Pd loading. Higher surface area carbons have less resistance to corrosion (as reported in Table 1 which compares

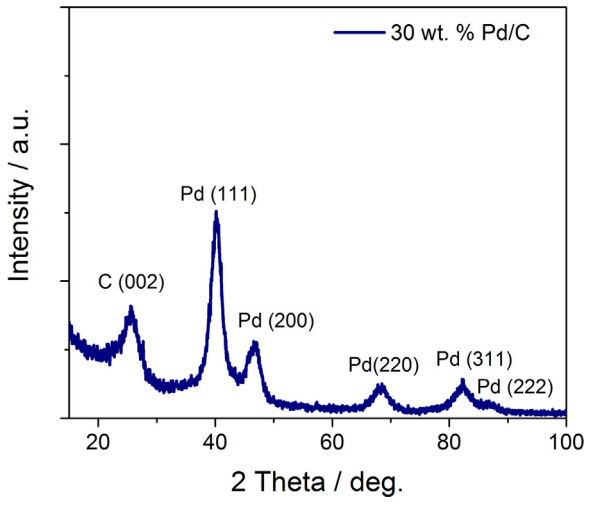

Fig. 1. XRD patterns for the 30 wt.% Pd/C catalyst.

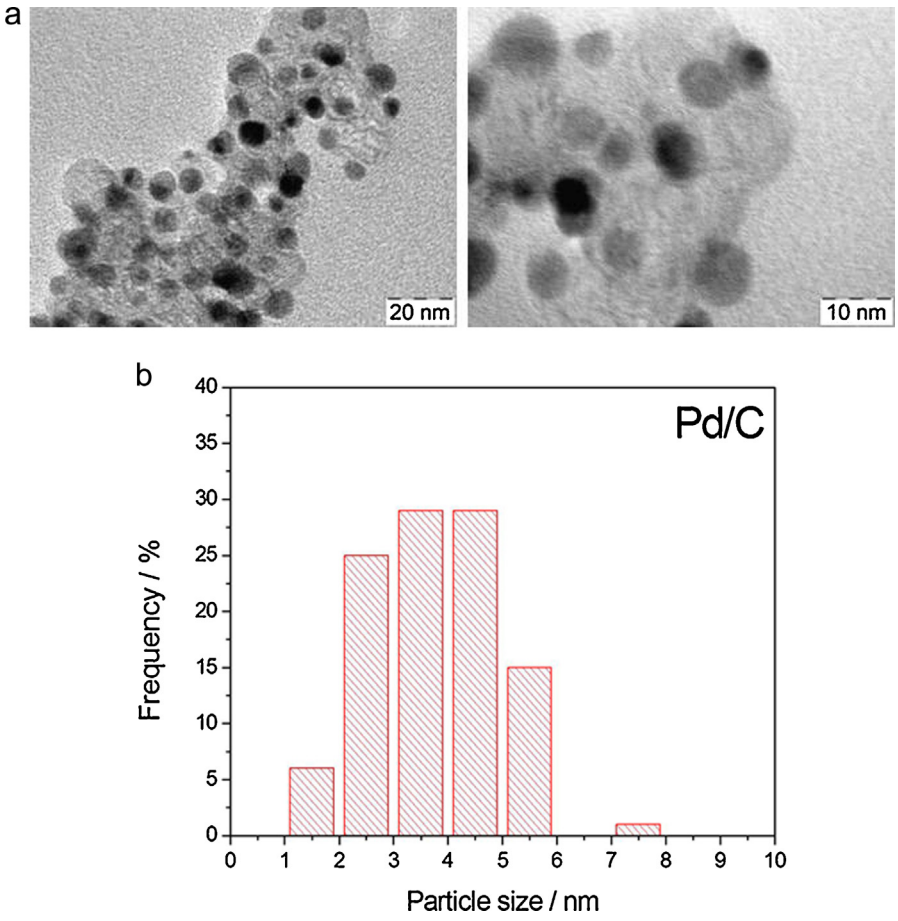

Fig. 2. a) TEM micrographs for the 30 wt.% Pd/C catalyst, at two different magnifications, and b) particle size histogram for the palladium particles.

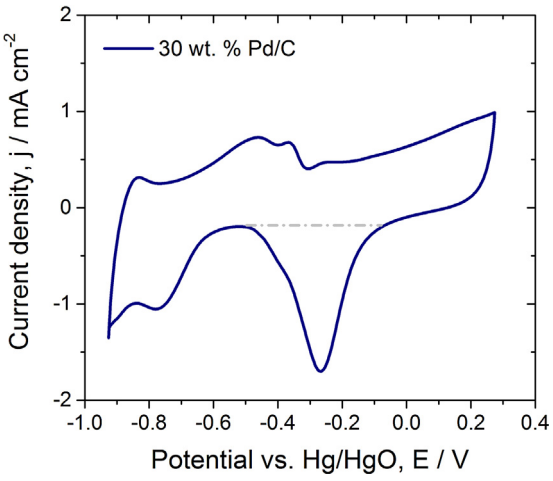

Fig. 3. Cyclic voltammogram for the catalyst 30 wt.% Pd/C. Measured at 20 mV s^{-1} in deaerated 1 mol dm^{-3} KOH solution.

C with C1), because a greater surface area is exposed to the KOH electrolyte. This has already been demonstrated in previous research comparing Pd supported on two different carbons: Vulcan (250 $m^2 g^{-1}$) and Kejtenblack (950 $m^{-2} g^{-1}$) [17]. Since the higher surface area carbons have less corrosion resistance in alkaline solution a compromise has been reached to use a medium-surface area carbon (220 $m^2 g^{-1}$) rather than a high-surface area carbon for the catalyst support. The gas diffusion layer carbon C1 had an even lower surface area (64 $m^2 g^{-1}$) which facilitates good corrosion resistance (Table 1); since no catalyst is loaded into this part of the electrode a high surface area was not necessary.

3.2. Internal structure of the gas diffusion electrode

The dimensions and composition of the 30 wt.% Pd/C gas diffusion electrode were studied using scanning electron microscopy (SEM). A cross-sectional area of a 1 cm^2 piece of the electrode was presented to the electron beam, so that the structure of the electrode could be clearly observed. The area presented to the electrode beam was the uncut edge that had not been subject to any forces other than the original hot-pressing. Fig. 4a shows the cross-section view of the electrode, with the separate layers labelled. The nickel mesh current collector is 0.05 mm thick, the 30 wt.% Pd/C catalyst layer presents an average thickness of 0.15 mm, and the C1 carbon / carbon cloth gas diffusion layer an

Table 1
Properties of the carbons C and C1 used for manufacturing the air electrode.

Carbon	S_{BET} / $m^2 g^{-1}$	Mass loss after 2 h at 0.5 V *vs.* Hg/HgO in 1 mol dm^{-3} KOH at 20 °C / % carbon
C	220	0.27
C1	64	0.06

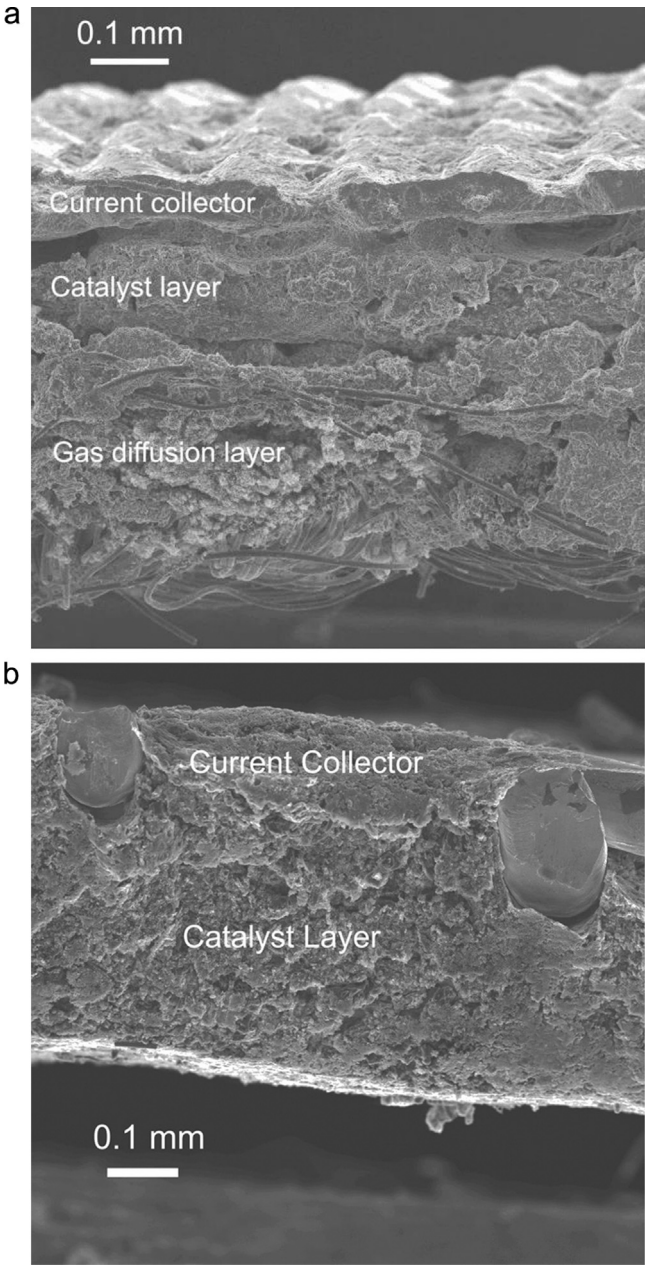

Fig. 4. Scanning electrode microscope cross-section of (a) 30 wt.% Pd/C gas diffusion electrode, and (b) Pt/C gas diffusion electrode (Gaskatel).

average thickness of 0.32 mm. This gives the electrode an overall thickness of 0.42 mm. The layers are well-adhered to each other; with a few small (< 0.05 mm) holes between the catalyst layer and the current collector (for example see the left-hand side of Fig. 4a). These holes are created during the hot-pressing, where uneven thermal expansion of the carbon-based catalyst layer and the current collector may cause some peeling of one layer from the other. This number of low-volume holes is not a great cause for concern, but they may cause localised disparities in current density distribution across the electrode surface. This could increase the rate of oxidative damage to the catalyst around the site of these holes.

A commercial Pt/C electrode, purchased from Gaskatel GmbH, in contrast, had an overall thickness of 0.5 mm (Fig. 4b). Unlike the Pd/C electrode, in the commercial electrode the catalyst layer occupies almost the entire volume of the electrode. The nickel current collector mesh is twice as thick as the one used in the Pd/C electrode but has a looser, woven structure (approximately 16 mesh size). Apart from a 2 mg cm^{-2} Pt loading, the exact composition and nature of the electrode materials were not made publically available, but EDX suggests that the electrode contains approximately 25 wt% PTFE and 6 wt% Pt.

Air electrodes ideally have a thickness of less than 0.5 mm, so that O_2 does not have to diffuse through a large volume of pores within the gas diffusion layer in order to reach the catalyst layer. The 30 wt.% Pd/C electrode thickness is compatible with other gas diffusion electrodes; both commercial and reported in the literature [38,39]. The air electrode used in a working iron-air battery built by the Swedish National Development Company, which was used for more than 1,000 charge-discharge cycles, had a thickness of 0.6 mm, and the cross-section of the electrode showed some small holes between layers, similar to Fig. 4 [40].

3.3. Performance of the gas diffusion electrode

The gas diffusion electrode was first studied using cyclic voltammetry in a 3-electrode glass cell with a 6 mol dm^{-3} KOH electrolyte at 20 °C. The cyclic voltammograms of the air electrode with the Pd/C catalyst were compared with cyclic voltamograms of two commercial electrodes (purchased from Johnson Matthey Fuel Cells and Gaskatel GmbH.) which use conventional Pt/C catalysts. The loading of Pd on the gas diffusion electrode was 0.5 mg cm^{-2}, compared with a loading of 2 mg cm^{-2} of Pt on the Gaskatel electrode, and 4 mg cm^{-2} of Pt on the Johnson Matthey (JM) electrode. Fig. 5 shows how the cyclic voltammograms of these three gas diffusion electrodes compare.

The Pd/C air breathing electrode shows superior performance to both the Gaskatel and JM electrodes for the oxygen reduction reaction (ORR), with an onset potential for oxygen reduction that is 60 mV more positive than the commercial electrodes (Table 2). However, the oxygen evolution reaction (OER) appears to have the lowest overpotential at the commercial Gaskatel electrode (see Table 2). The Gaskatel electrode also has the highest current density for oxygen evolution at the cutoff potential of +0.6 V vs. Hg/HgO; the current density is 75 mA cm^{-2} compared to 13 mA cm^{-2} for the Pd/C air electrode. As the exact composition of the Gaskatel electrode is not known, it is not possible to say why the OER performance is superior; there may be additional additives in the electrode that improve oxygen evolution, for example certain

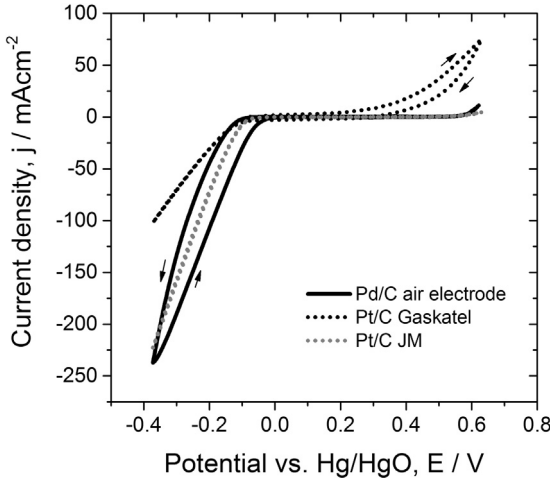

Fig. 5. Cyclic voltammograms of Pd/C electrode and Pt/C commercial gas diffusion electrodes. The electrolyte was 6 mol dm^{-3} KOH solution, and the oxygen flow into the back of the electrodes was 100 cm^3 min^{-1}. The oxygen outlet was open to the atmosphere such that the back of the electrode was under no additional pressure. Abbreviation JM = Johnson Matthey.

Table 2
Onset potentials for oxygen reduction and evolution at the gas diffusion electrodes.

Electrode	E(ORR) / V *vs.* Hg/HgO	E(OER) / V *vs.* Hg/HgO
Pd/C	+0.01	+0.54
Pt/C (Gaskatel)	−0.05	+0.15
Pt/C (JM)	−0.05	+0.57

carbon and nickel additives could improve the OER performance [41].

However, the durability of the air electrodes after lengthy periods of cycling at high current densities is also important; the most active catalysts are not always necessarily the most stable. For this reason, the effect of repeated charge–discharge cycles at constant current on the air electrodes was studied. It is already known that the Johnson Matthey electrode is not a suitable bifunctional gas diffusion electrode, as it does not function well for oxygen evolution during charging due to a high rate of carbon oxidation [42]. Therefore, the charge-discharge profiles of the Pd/C air electrode were compared with the Pt/C electrode from Gaskatel only, as this electrode has superior bifunctionality. Both electrodes were studied at a range of current densities (10–80 mA cm^{-2}) and temperatures (20–80 °C).

Fig. 6 shows the results of a short duration experiment to characterise the charge-discharge performance of both electrodes with one hour cycles under variable current density. In the range 10-50 mA cm^{-2} the commercial Pt/C electrode showed a lower OER potential, but at 80 mA cm^{-2} the Pd/C electrode outperformed the commercial electrode, by having a more stable and lower average OER potential during the thirty minutes charging. The Pd/C electrode outperforms the commercial Pt/C electrode for the ORR at all current densities: the difference in ORR potential between the two electrodes increases with increasing current density, and at 80 mA cm^{-2} the ORR potential was −0.25 V vs. Hg/HgO for the Pd/C electrode compared with −0.54 V vs. Hg/HgO for the Pt/C electrode.

These results indicate that the Pd/C electrode is superior for metal-air batteries, where the ORR potential needs to be as high as possible, and also that the Pd/C electrode is more stable upon cycling at higher current densities. Following on from these results, more long-term charge–discharge tests were performed to determine the long-term stability of the Pd/C electrode.

The results of repeated charge-discharge cycling of both electrodes at a modest current density (20 mA cm^{-2}) for four days can be seen in Fig. 7. The Pd/C electrode adopted a stable charge–discharge profile after 40 hours of cycling (each cycle was 4 hours long in this case). There was an improvement in OER performance; at the start of cycling the potential was +0.64 V and by the end it was +0.60 V vs. Hg/HgO. The same cannot be said for the discharge ORR cycles, which deteriorated from −0.09 V to −0.22 V vs. Hg/HgO. The commercial Pt/C electrode (Gaskatel) did not show the same degree of durability: although the OER potential was stable and actually lower than at the Pd/C electrode throughout the test, the ORR potential decreased rapidly compared with the Pd/C electrode, and after 44 hours it reached the lower cut-off potential of −0.5 V vs. Hg/HgO that was set for this experiment. During the test, the electrolyte solution around the Pt/C electrode gradually turned brown, whereas for the Pd/C electrode it turned only slightly yellow: this suggests a deeper degree of carbon corrosion at the Pt/C electrode. The fine nickel mesh (32 mesh hole size) may have a protective role in holding the electrode together and delaying loss of carbon into the solution, as well as contributing to the OER reaction: the presence of nickel was known to stabilise the OER reaction in previous work carried out on a bifunctional air electrode [32].

Ultimately, to be useable in a rechargeable metal-air battery, an air electrode must have a lifetime of at least 1,000 cycles, preferably more. Running an experiment with 4 hour charge-discharge cycles is impractical, as 1,000 cycles would take almost 6 months. However, the electrode suffers some damage (e.g. oxidation, shape change of particles, dissolution) at the early part of each cycle in switching from positive to negative current and vice versa, so it should be possible to get an impression of the longevity of the electrode by running many shorter cycles. Fig. 8 shows the results of 1,000 charge–discharge cycles of 5 minutes each, on a fresh piece of the Pd/C air electrode.

The electrode showed a remarkable degree of stability in OER potential, which even decreased after the first couple of hours of cycling. At the start of cycling the potentials at 10 mA cm^{-2}, the charging and discharging potentials were +0.55 and −0.07 V vs. Hg/HgO respectively. After 1,000 cycles the potentials were +0.54 and −0.23 V vs. Hg/HgO. Thus, the Pd/C electrode is very stable towards recharging, and even shows a slight increase in performance after several days cycling. On the other hand, the discharging ORR

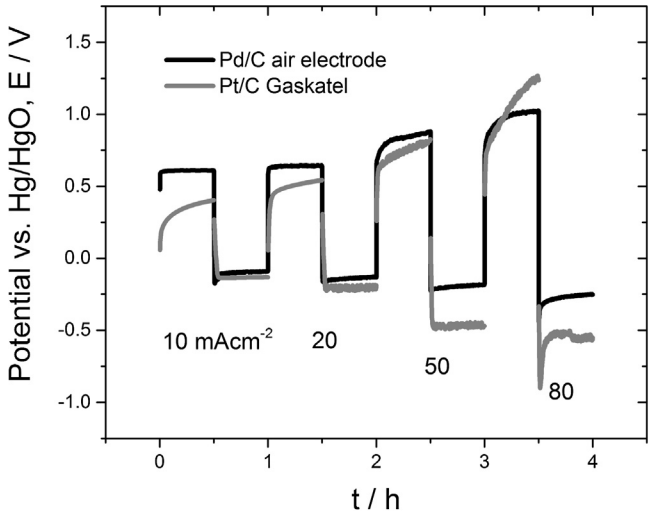

Fig. 6. Charge–discharge profiles of Pd/C air electrode compared with Pt/C electrode (Gaskatel GmbH). The variable current densities used for cycling are labelled on the graph. The electrolyte was 6 mol dm^{-3} KOH at 20 °C. The oxygen flow rate into the back of the air electrode was 100 cm^3 min^{-1} under atmospheric pressure.

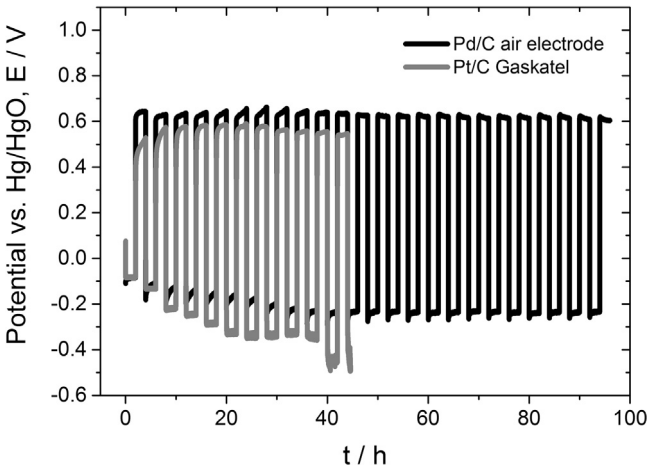

Fig. 7. Charge/discharge profiles of Pd/C air electrode and Gaskatel Pt/C air electrode at 20 mA cm^{-2} current density, at 20 °C in 6 mol dm^{-3} KOH, with 100 cm^3 min^{-1} rate of oxygen flow into the back of the air electrode.

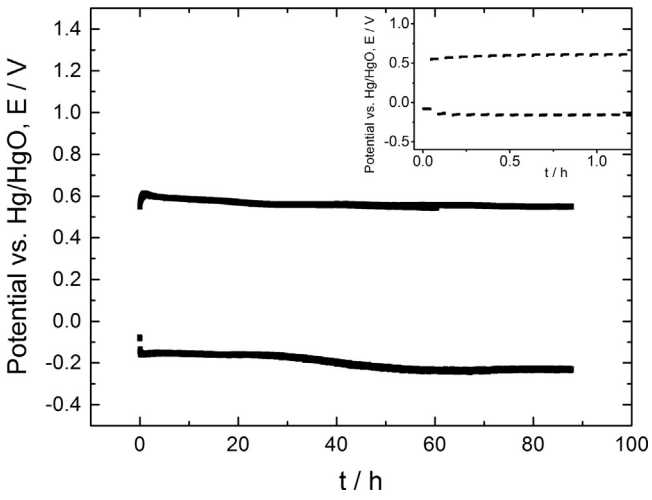

Fig. 8. Charge–discharge profiles of Pd/C during 1,000 cycles of 5 minutes duration. The graph inset shows the first hour of cycling. There are no lines between data points, in order to improve clarity as separate cycles are very close together on the graph. The cycling current density was 10 mA cm^{-2}, the electrolyte was 6 mol dm^{-3} KOH, with 100 cm^3 min^{-1} rate of oxygen flow into the back of the air electrode.

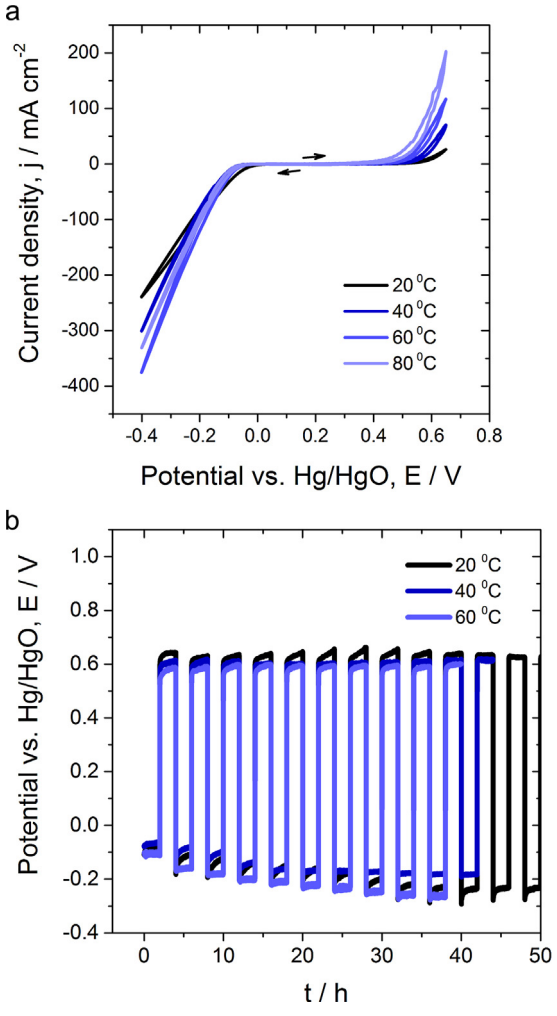

Fig. 9. a) Cyclic voltammograms, and b) charge–discharge profiles at 20 mA cm^{-2} of Pd/C at different temperatures, at 20 mA cm^{-2} current density, at 20 °C in 6 mol dm^{-3} KOH, with 100 cm^3 min^{-1} rate of oxygen flow into the back of the air electrode.

performance decreased by 0.16 V over the cycling. Much of this decrease occurred over the 25–45 hour period, which correlates with the results in Fig. 4. It appears that after the first 40–50 hours of cycling the ORR performance of the electrode stabilises, irrespective of the length and number of the cycles.

Finally, the effect of temperature on the Pd/C air electrode was studied. Fig. 9 shows cyclic voltammograms and charge-discharge profiles of the Pd/C electrode in the temperature range 20–80 °C. Cyclic voltammetry (Fig. 9a) showed that the OER current density increases with temperature as the reaction rate increased, reaching a cutoff value of 200 mA cm^{-2} at 80 °C compared to only 30 mA cm^{-2} at 20 °C. The increase in the OER and ORR currents shows a linear trend between 20 and 60 °C, but the ORR current decreases slightly from 60 to 80 °C, which is probably due to an increased rate of oxidative damage to the Pd/ C at increased temperature during cycling.

The Pd/C electrode showed the optimum bifunctionality at 60–80 °C, with only 0.5 V potential difference between ORR and OER. However, the charge-discharge profiles (Fig. 9b) show that upon repeated cycling at 60 °C, the ORR potential of the air electrode is less stable than at 20–40 °C during the first 10 cycles, in particular showing a large decrease in ORR potential after the first cycle. Therefore, the recommended operating temperature of the air electrode would be approximately 40 °C, as this temperature showed the best bifunctionality by the 10th charge–discharge cycle (Fig. 9b).

4. Conclusions

An oxygen gas diffusion electrode including a 30 wt.% Pd/C catalyst, with a carbon-based gas diffusion layer and nickel mesh current collector has been constructed by hot-pressing. The electrode has good bifunctional properties, with 0.53 V potential difference between the onset of oxygen reduction (discharge) and evolution (charge). It has a promising long-term stability, and still functions after 1,000 charge–discharge cycles at 10 mA cm^{-2}, as well as after 96 hours (4 days) of cycling at 20 mA cm^{-2}.

The durability and bifunctionality of the Pd/C electrode at modest and high current densities (20-80 mA cm^{-2}) is superior to two commercially-produced Pt/C gas diffusion electrodes, from Gaskatel and Johnson Matthey, with precious metal loadings of 2 mg cm^{-2} and 4 mg cm^{-2} respectively. The Pd/C air electrode therefore makes efficient use of the small 0.5 mg cm^{-2} precious metal loading, due to its well-dispersed, nanoscale particles. The rate of oxygen evolution and reduction increases linearly with temperature between 20 and 60 °C, but there is a decrease in the durability of the electrode above 40 °C.

Acknowledgements

This work was enabled by an EU grant FP7 (NECOBAUT Grant agreement no. 314159).

References

[1] A.F. Burke, Advanced Batteries for Vehicle Applications, Encyclopaedia of Automotive Engineering, Wiley, 2014, pp. 1–20.
[2] J.S. Lee, S.T. Kim, R. Coa, N.S. Choi, M. Liu, K.T. Lee, J. Cho, Metal-air batteries with high energy density: Li-air versus Zn-air, Adv. Energy Mater. 1 (2010) 34–50, doi:http://dx.doi.org/10.1002/aenm.201000010.
[3] Q. Wang, P. Ping, X. Zhao, G. Chu, J. Sun, C. Chen, Thermal runaway caused fire and explosion of lithium ion battery, Journal of Power Sources 208 (2012) 210–224, doi:http://dx.doi.org/10.1016/j.jpowsour.2012.02.038.
[4] X. Li, D. Pletcher, C. Ponce de Léon, F.C. Walsh, R.G.A. Wills, Redox flow batteries for energy storage using zinc electrodes, in: C. Menictas, M. Skyllas-Kazacos, T. M. Lim (Eds.), Ch. 6 in Advances in batteries for large- and medium-scale energy storage: Applications in power systems and electric vehicles, Woodhead, 2015, pp. 293–315.

[5] M. Chen, Rechargeable metal-air electrochemical cells with recharging electrode and separator in ionic communication with the electrodes, PCT Int Appl. (2002) WO 2002058171 A2 20020725.
[6] H. Ohkuma, I. Uechi, M. Matsui, Y. Takeda, O. Yamamoto, N. Imanishi, Journal of Power Sources 245 (2014) 947–952, doi:http://dx.doi.org/10.1016/j.jpowsour.2013.06.146.
[7] S. Zhang, H. Zhang, S. Liu, F. Tu, W. Zhang, C. Zhao, Int. J. Electrochem. Sci. 9 (2014) 1690–1701.
[8] M. Yuasa, M. Nishida, T. Kida, N. Yamazoe, K. Shimanoe, J. Electrochem. Soc. 158 (2011) A605–A610.
[9] C. Zhu, A. Nobuta, I. Makatsugawa, T. Akiyama, Int. J, Hydrogen Energ . 38 (2013) 13238–13248.
[10] K. Jung, J. Jung, W.B. Im, S. Yoon, K. Shin, J. Lee, Appl. Mater. Interfaces 5 (2013) 9902–9907.
[11] O. Savadogo, K. Lee, K. Oishi, S. Mitsushima, N. Kamiya, K.I. Ota, Electrochem. Commun. 6 (2004) 105–109, doi:http://dx.doi.org/10.1016/j.elecom.2003.10.020.
[12] H. Erikson, A. Kasikov, C. Johans, K. Kontturi, K. Tammeveski, A. Sarapuu, Journal of Electroanalytical Chemistry 652 (1-2) (2011) 1–7, doi:http://dx.doi.org/10.1016/j.jelechem.2010.12.021.
[13] G.F. Alvarez, M. Mamlouk, K. Scott, International Journal of Electrochemistry 2011 (2011) 684535, doi:http://dx.doi.org/10.4061/2011/684535.
[14] M. Shao, T. Yu, J.H. Odell, M. Jin, Y. Xia, Chem. Commun 47 (2011) 6566–6568, doi:http://dx.doi.org/10.1039/C1CC11004G.
[15] O. Outiki, E. Lamy-Pitara, J. Barbier, Reaction Kinetics and Catalysis Letters 23 (3-4) (1983) 213–220.
[16] L. Trung-Phuoc, C. Pham-Huu, V. Da Costa, I. Janowska, Chem. Commun. 50 (4435) (2014) 14433–14435.
[17] C. Alegre, A. Stassi, E. Modica, C. Lo Vecchio, A.S. Arico, V. Baglio, RSC Adv. 5 (2015) 25424–25427, doi:http://dx.doi.org/10.1039/C4RA15578E.
[18] F.W.T. Goh, Z. Lui, X. Ge, Y. Zong, G. Du, T.S.A. Hor, Electrochim. Acta 114 (2013) 598–604.
[19] Z. Zhang, X. Wang, G. Cui, A. Zhang, X. Zhou, H. Xu, L. Gu, Nanoscale 6 (2014) 3540–3544.
[20] Y. Xie, H. Li, C. Tang, S. Li, J. Li, Y. Lv, X. Wei, Y. Song, J. Mater. Chem. A 2 (2014) 1631–1635.
[21] X. Sun, P. Song, Y. Zhang, C. Liu, W. Xu, W. Xing, Scientific Reports 3 (2505) (2013) 1–5.
[22] Y. Lee, J. Suntivich, K.J. May, E.E. Perry, Y. Shao-Horn, J. Phys. Chem. Lett. 3 (2012) 399–404.
[23] N. Sasikala, K. Ramya, K.S. Dhathathreyan, Energy Conservation Management 77 (2014) 545–549.
[24] J.C. Calderón, N. Mahata, M.F.R. Pereira, J.L. Figueiredo, V.R. Fernandes, C.M. Rangel, L. Calvillo, M.J. Lázaro, E. Pastor, International Journal of Hydrogen Energy 37 (8) (2012) 7200–7211.
[25] B. Avasarala, R. Moore, P. Haldar, Electrochimica Acta 55 (2010) 4765–4771, doi:http://dx.doi.org/10.1016/j.electacta.2010.03.056.
[26] M. Neal Golovin, I. Kuznetsov, I. Atijosan, L.A. Tinker, C.S. Pedicini, MRS Proceedings 496 (1997) 43, doi:http://dx.doi.org/10.1557/PROC-496-43.
[27] T. Engl, L. Gubler, T.J. Schmidt, J. Electrochem. Soc. 162 (2015) F291–F297, doi:http://dx.doi.org/10.1149/2.0681503jes.
[28] M. Brodt, T. Han, N. Dale, E. Niangar, R. Wycisk, P. Pintauro, J. Electrochem. Soc. 162 (1) (2015) F84–F91.
[29] A. Stassi, I. Gatto, V. Baglio, A.S. Aricò, International Journal of Hydrogen Energy 39 (2014) 21581–21587, doi:http://dx.doi.org/10.1016/j.ijhydene.2014.05.090.
[30] A.S. Aricò, V. Baglio, A. Di Blasi, E. Modica, P.L. Antonucci, V.J. Antonucci, Electroanal. Chem. 557 (2003) 167–176.
[31] R. Pattabiraman, Applied Catalysis A: General 153 (1997) 1–20.
[32] S.S. Dipti, U.C. Chung, W.S. Chung, Metals and Materials International 13 (5) (2007) 417–420.
[33] S. Trasatti, O.A. Petrii, Real surface area measurements in electrochemistry, Pure and Applied Chemistry 63 (5) (1991) 731–734.
[34] A.N. Correia, L.H. Mascara, S.A.S. Machado, L.A. Avaca, Active surface area determination of Pd-Si alloys by H-adsorption, Electrochimica Acta 42 (3) (1997) 493–495.
[35] W.G. Hardin, D.A. Slanac, X. Wang, S. Dai, K.P. Johnston, K.J. Stevenson, J. Phys. Chem. Lett 4 (2013) 1254–1259.
[36] S. Song, H. Zhang, X. Ma, Z.G. Shao, Y. Zhang, B. Yi, Electrochemistry Communications 8 (2006) 399–405.
[37] M. Hamdani, R.N. Singh, P. Chartier, Int. J. Electrochem. Sci. 5 (2010) 556–577.
[38] M. Mortazavi, K. Tajiri, J. Fuel Cell Sci. Technol. 11 (2) (2013) 021002.
[39] K. Tsubosaka, R. Fujito, K. Fujii, Gas diffusion layer for fuel cell, fuel cell, and method of manufacturing gas diffusion layer for fuel cell, PCT Int, Appl. (2013) WO 2013117974 A1 20130815.
[40] L. Carlsson, L. Öjefors, J. Electrochem. Soc. 2 (1980) 525–528.
[41] J. Wang, H. Zhong, Y. Qin, X. Zhang, Angewandte Chemie 52 (2013) 5248–5253, doi:http://dx.doi.org/10.1002/anie.201301066.
[42] X. Li, D. Pletcher, A.E. Russell, F.C. Walsh, R.G.A. Wills, S.F. Gorman, S.W.T. Price, S.J. Thompson, Electrochem. Comm. 34 (2013) 228–230, doi:http://dx.doi.org/10.1016/j.elecom.2013.06.020.